Geophys. J. Int. (2006) doi: 10.1111/j.1365-246X.2006.03146.x

Broad-band observations of earthquake-induced rotational ground motions

Heiner Igel,[1] Alain Cochard,[1,*] Joachim Wassermann,[1] Asher Flaws,[1,3]† Ulrich Schreiber,[2] Alex Velikoseltsev[2] and Nguyen Pham Dinh[1]

[1]*Department of Earth and Environmental Sciences, Ludwig-Maximilians-University Munich, Theresienstraße* 41, D-80333 *Munich, Germany. E-mail: heiner.igel@geophysik.uni-muenchen.de*

[2]*Forschungseinrichtung Satellitengeodäsie, Technical University Munich, Fundamentalstation Wettzell, Sackenriederstrasse* 25, D-93444 *Kötzting, Germany*

[3]*Department of Physics and Astronomy, University of Canterbury,* Private Bag 4800, *Christchurch, New Zealand*

Accepted 2006 July 16. Received 2006 July 16; in original form 2006 May 24

SUMMARY

It has been noted by theoretical seismologists for decades that—in addition to translations and strains—the rotational part of ground motions should also be recorded. It is expected that collocated measurements of translations and rotations may (1) allow transformation of translational seismograms to the complete ground motion of an observation point; (2) help to further constrain rupture processes and (3) provide additional hazard-relevant information to earthquake engineers. The lack of instrumental sensitivity used to be the main obstacle to observing rotational motions. Recently, ring laser technology has provided the means to develop instruments that allow in principle the observation of rotational motions in a wide frequency band and epicentral distance range. Here we investigate whether this technology—originally designed for geodesy—is capable of providing accurate and useful observations for seismology. We report observations of rotations around a vertical axis of several earthquakes obtained by a 4×4 m ring laser installed in SE-Germany and compare them to collocated broad-band translations. Assuming plane transverse wave propagation, acceleration and rotation rate should be in phase and their amplitude ratio proportional to horizontal phase velocity. Here we show that most of the observations can be explained under these assumptions and that the collocated observations allow the estimation of wavefield properties (e.g. phase velocities, propagation directions), otherwise only accessible through seismic array measurements, polarization analysis, or additional strain measurements.

Key words: broad-band sensor, ring laser, rotational ground motions, seismic instrumentation.

INTRODUCTION

Seismology is a science primarily based on the observation, processing and inversion of three-component translational ground motions (displacement, velocity, or acceleration recorded in three orthogonal directions, usually, N–S, E–W and vertical). It is well known that—in addition to translations—three components of rotations should also be measured (theoretically allowing the reconstruction of the complete motion of a measurement point, e.g. Aki & Richards 2002; Trifunac & Todorovska 2001; Graizer 2005, 2006). Inertial sensors commonly used in seismology are sensitive to, and thus polluted by rotational motions, increasing observational uncertainties. Furthermore, sensors that measure the horizontal components of rotation at the surface (tiltmeters) are sensitive to translational motions. As noted by Aki & Richards (2002, p. 608), seismology still awaits a suitable instrument to make rotational measurements with similar sensitivity as in classical broad-band seismology.

In the past decades several attempts have been made to build rotational sensors and observe earthquake- (or explosion-) induced ground motions. Mechanical devices, fibre-optical technology or solid-state sensors were used to observe rotational ground motions close to sources of seismic energy (Farrell 1969; Nigbor 1994; Takeo & Ito 1997), but did not have the sensitivity for observations of more distant events. In several studies the rotational components of motion were derived from appropriately sized seismic arrays (Spudich *et al.* 1995; Singh *et al.* 1997; Huang 2003), but never compared to direct measurements of rotations until recently (Suryanto *et al.*

*Now at: Ecole et Observatoire des Sciences de laTerre, Institut de Physique du Globe, 5 rue René Descartes, F-67084 Strasbourg Cedex, France.

†Now at: Department of Physics, Technical University Munich, James Franck Str. 85748 Garching, Germany.

COLOUR FIG.

Figure 1. Left: Ring laser (G-ring) installed at the Wettzell observatory, SE-Germany. The G-ring has a side length of 4 m. The picture shows the tubes containing the lasing gas and the corners with the reflecting mirrors. Right: Ring laser measurement principle. Two counter-rotating single-mode laser beams interfere to generate a beating in case the system rotates with respect to the surface normal. The beating frequency is directly proportional to rotational velocity.

2006a), when array-derived rotations were observed to match direct measurements to within a few percent. Finally, high-sensitivity ring laser technology (e.g. Stedman *et al.* 1995; Stedman 1997) that was developed for geodetic purposes in the past decades (e.g. Rautenberg *et al.* 1997; Schreiber *et al.* 2003a, 2004) led to the detection of earthquake-induced ground motions far from seismic sources (Stedman *et al.* 1995; McLeod *et al.* 1998; Pancha *et al.* 2000), opening a new direction in seismic instrumentation. After a pioneering numerical study of rotations (Bouchon & Aki 1982), the fundamental solutions for the displacement field from a double-couple point source were expressed for rotations and divergence (Cochard *et al.* 2006). In this study, our focus is on the vertical component of rotation (sometimes also called twist, yaw, spin or torsion in engineering applications i.e. the rotation around a vertical axis) as this is the motion component our ring laser instrument is recording.

Following the above mentioned first observations of distant earthquake-induced rotations, the ring laser technology and data acquisition system was continuously improved and modified to fulfil the needs of seismology. This implies particularly precise timing and observations at sufficiently high sampling rate (Schreiber *et al.* 2005a,b). Those modifications were carried out on the 4 × 4 m ring laser system that was installed at the geodetic observatory Wettzell, SE-Germany in 2002 (Fig. 1, left), which is also the location of a seismic broad-band sensor (WET) of the German Regional Seismic Network (GRSN). These collocated sensors have observed ground motions (almost) permanently ever since, allowing us to extract a data base with several dozens of earthquake events of various epicentral distances and magnitudes. At the onset of this study there were several open questions:

(1) Is the sensor sensitivity enough to observe teleseismic signals?

(2) Are the observed signals consistent in waveform and amplitude with the collocated measurements of translations?

(3) Does local structure and/or the specific sensor installation in a specially designed cave affect the observations (as is well known for tilt and strain measurements)?

(4) How do the observations vary with epicentral distance and magnitude?

(5) Is a sufficiently broad frequency band observed to allow comparison with translations?

(6) Can we extract additional information from both types of observations?

The main goal of this paper is to present observations from several earthquakes with the aim of verifying the potential of ring laser (or more general optical) sensors to accurately observe rotations, and to discuss future applications in seismology.

This study builds on the pioneering first observations made by Stedman *et al.* (1995), McLeod *et al.* (1998) and Pancha *et al.* (2000) who studied observations made with the ring lasers installed in Christchurch, New Zealand. They were the first to exploit the simple relationship between transverse acceleration and rotation rate assuming plane horizontally polarized wave propagation. Nevertheless their observations were not fully consistent, and were only studied in a narrow frequency band. The first detailed analyses of collocated observations of transverse acceleration and rotation rate were carried out by Igel *et al.* (2005) and Cochard *et al.* (2006). They showed that for several distant large earthquakes the waveforms and amplitudes of translations and rotations matched the expected behaviour assuming plane wave theory. In addition, 3-D synthetic modelling showed that it seems possible to use the collocated observations to estimate horizontal phase velocities with surprising accuracy. This paper focuses entirely on observations and aims at extending the previous studies to a wide range of epicentral distances and magnitudes, proposing processing tools that can be used to analyse rotations and translations and identifying observational aspects that need to be explained with synthetic modelling tools and/or theoretical developments.

ROTATION SENSORS

In this section we briefly review the state of the art of rotational sensors and provide details on the ring laser system with which our observations were carried out. There are basically four types of sensors that have been used to observe rotations:

(1) mechanical sensors (e.g. Moriya & Marumo 1998; Teisseyre *et al.* 2003) that exploit the differential measurements of two or more translational sensors;

(2) solid-state sensors as used by Nigbor (1994) and Takeo *et al.* (1998). This sensor type contains a vibrating quartz tuning fork and exploits Coriolis forces;

Table 1. List of earthquakes that were used in this study. The signal-to-noise ratio (S/N) for transverse accelerations and rotation rate are shown along with horizontal phase velocity estimates based on peak amplitude ratios. The zero-lag cross-correlation coefficient is a measure of waveform fit between transverse acceleration and rotation rate (1.0 corresponding to perfect fit). See text for details.

Date	Time (UTC)	Lat(°)	Lon (°)	Mag(L,b,S,w)	Region	S/N (Acc.) *1e-3	S/N (Rot.)	Phase vel. (m s^{-1})	Peak Corr. Coeff.
03/05/21	18:44:20	36.964	003.634	6.9	Algeria	295	5341	2886	0.63
03/05/26	09:24:33	38.849	141.568	7.0	Honshu	45.7	67	4225	0.49
03/07/06	19:10:33	40.340	026.070	5.7	Turkey	575	187	3832	0.997
03/08/14	05:14:55	39.193	020.741	6.3	Greece	2371	1351	3137	0.96
03/09/25	19:50:06	41.781	143.903	8.3	Hokkaido	3320	16570	4426	0.997
03/09/27	11:33:24	50.012	087.824	7.5	Siberia	3357	3337	3714	0.98
03/09/27	18:52:53	50.060	087.690	6.6	Siberia	218	303	3528	0.98
03/10/01	01:03:25	50.218	087.685	7.1	Siberia	1012	1659	3428	0.99
03/10/31	01:06:40	37.890	142.680	7.0	Honshu	5.8	22	3648	0.93
03/11/17	06:43:31	51.140	177.860	7.8	Rat Island	206	27	3570	0.62
04/02/05	21:05:12	−03.620	135.530	7.1	Irian Jaya	0.218	17	3836	0.97
04/02/07	02:42:43	−04.030	134.780	7.5	Irian Jaya	8.233	22	4232	0.95
04/02/24	02:27:53	35.290	−003.840	6.4	Gibraltar	1.66	260	3580	0.994
04/03/17	03:21:12	−21.100	−065.560	6.1	Bolivia	2.8	30	2964	0.59
04/04/05	21:24:06	36.590	070.850	6.6	Afghanistan	1.8	14.9	3832	0.92
04/05/29	20:56:14	34.220	141.790	6.6	Honshu	17.6	122	3241	0.994
04/12/05	01:52:37	48.120	008.080	5.0	Germany	47.7	90	2253	0.84
04/12/26	00:58:53	03.300	095.980	9.0	Sumatra	34 318	485	1836	0.989

(3) fibre-optic gyros based on coiled long optical fibres (e.g. Levevre 1993) and

(4) ring laser based sensors (e.g. Stedman *et al.* 1995; Stedman 1997; Schreiber *et al.* 2005, 2006).

The most important property that makes a rotation sensor useful for seismology is its resolving power of rotational motions around the corresponding axes and the insensitivity to translational motions. The rotation rates to be expected in seismology range from a few deg s^{-1} (e.g. Nigbor 1994) close to seismic sources to 10^{-11} rad s^{-1} observed for large earthquakes at teleseismic distances (e.g. Igel *et al.* 2005; Schreiber *et al.* 2005, 2006), thus spanning more than 10 orders of magnitude. It is unlikely that one instrument (or one instrumental technology) will ever be capable of providing accurate measurements over such a large range of amplitudes. Therefore, it is likely that different technologies shall be applied to strong ground motion observations and teleseismic observations as is the case in classical seismology.

In this study we present observations using a ring-laser based rotation sensor with currently the highest sensitivity. This has the advantage that we can observe rotations over a wide amplitude range, including teleseismic events, and we can investigate the observations in the context of plane wave theory thereby verifying the consistency of the recording technology by comparison with classical seismic broad-band measurements.

RING LASER MEASUREMENT PRINCIPLE

Ring lasers detect the Sagnac beat frequency of two counter-propagating laser beams (Stedman 1997; see Fig. 1, right). These active interferometers are realized by triangular or (in our case) square closed cavities in which the light beams interfere. If this instrument is rotating on a platform with respect to inertial space, the effective cavity length between co-rotating and counter-rotating laser cavity differs and one obtains a frequency splitting (and thus a beating pattern) of the resulting standing wave. This beat frequency δf is directly proportional to the rotation rate Ω around the surface normal $\mathbf{n}$ of the ring laser system as given by the Sagnac equation

$$\delta f = \frac{4A}{\lambda P}\mathbf{n}\cdot\Omega, \tag{1}$$

where P is the perimeter of the instrument, A the area, and λ the laser wavelength. This equation has three contributions that influence the beat frequency δf :

(1) Variations of the scale factor ($4A/\lambda P$) have to be avoided by making the instrument mechanically as rigid and stable as possible;

(2) changes in orientation $\mathbf{n}$ enter the beat frequency via the inner product and

(3) variations in $\mathbf{\Omega}$ (e.g. due to changes in the Earth's rotation rate, or seismically induced rotations) are representing the most dominant contribution to δf.

Note that translations do not generate a contribution to the Sagnac frequency. Ring lasers are sensitive to rotations only, given stable ring geometry and lasing. The second effect implies that for coseismic observations at the Earth's surface the horizontal components of rotation (i.e. tilt) will contribute to the vertical component of rotation rate. This contribution was investigated by McLeod *et al.* (1998) and Schreiber *et al.* (2005, 2006) who concluded that it is one to two orders of magnitude lower than the rotation due to the seismic signal. At present it is not clear whether standard tiltmeters are providing accurate enough information in the relevant frequency band as their signals are polluted by transverse acceleration. This is currently being investigated. In this study, the rotational observations are not corrected for tilt.

The ring laser used in this study (named G, Fig. 1, left) is a He–Ne-gas laser with a high Q cavity and a surface area of 16 m^2. It operates on a laser wavelength of 633 nm. It is mounted horizontally in the Geodetic Fundamentalstation Wettzell, SE-Germany, at a latitude of 49.15° north – resulting in the Sagnac frequency induced by the Earth's rotation of 348.6 Hz, sampled at 1000 Hz. This signal is frequency modulated by any additional rotational motions (e.g. due to a passing seismic wavefield). The instrumental sensitivity of ring lasers is limited by the scale factor and quantum noise processes.

COLOUR FIG.

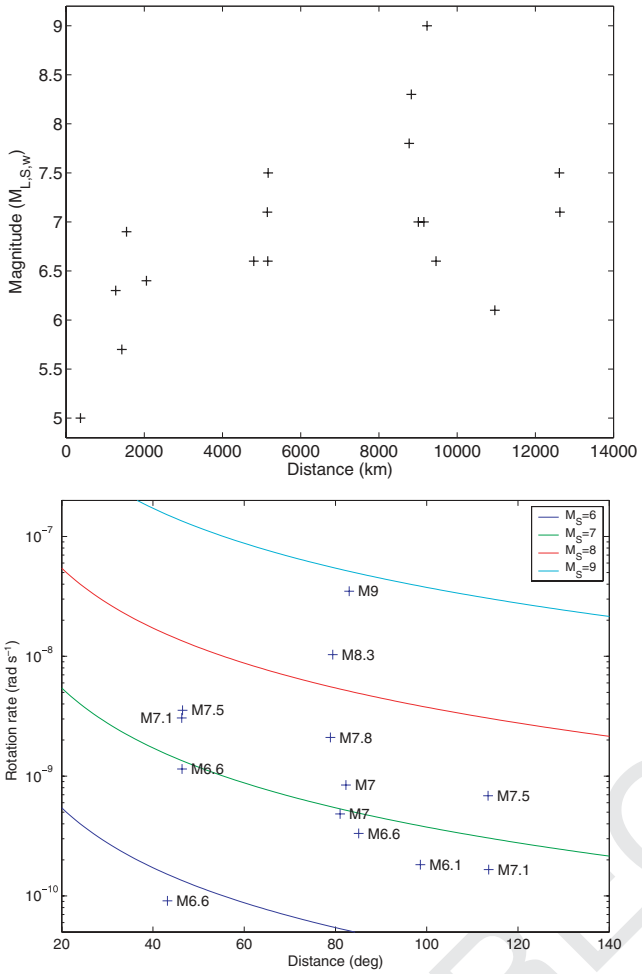

Figure 2. Top: Magnitude (MS, ML, Mb or Mw as given in data base) distribution of processed events as a function of epicentral distance. Bottom: Peak rotation rates in a narrow frequency band (dominant period $T = 30$ s) for events between 20°–140° distance compared to predictions for M6-M9 based on the definition of the surface wave magnitude.

With the G ring laser, rotation rates as small as 10^{-10} rad s$^{-1}/\sqrt{\text{Hz}}$ can be observed (Schreiber *et al.* 2003b). Ring lasers rigidly attached to bedrock allowed the detection of small changes of the orientation of the surface normal caused by solid earth tides, ocean loading (Schreiber *et al.* 2003a) and diurnal polar motion (Schreiber *et al.* 2004).

In terms of sensor sensitivity and temporal stability, the most important factors are the ring laser geometry [through eq. (1)], the quality of the mirrors, the stability of temperature and atmospheric pressure at the recording site, and quantum noise processes that limit the dynamic range for small rotations. As it is located in a purpose-built observatory and installed on an extremely stiff material (Zerodur¨), pollution due to temperature, pressure or deformation can be neglected. Further details on the recording technology, the acquisition system, and instrument sensitivity can be found in Schreiber *et al.* (2006). A modified ring laser system was recently designed specifically for seismological applications (Schreiber *et al.* 2005) and two prototypes installed at different locations (one horizontally at Pinon flat observatory, California, the second vertically in a building of Christchurch University, New Zealand). The (soft) infrastructure to gather the observations from the increasing number of high-sensitivity ring laser systems worldwide that are currently being built should allow future comparative studies of the observed rotational ground motions.

ROTATION DATA BASE AND PRE-PROCESSING

The G-ring at the Fundamentalstation, Wettzell, SE-Germany, was installed in 2002. As the sensor was primarily developed for geodetic purposes with sampling rates below 1 Hz and averaging over several seconds, the acquisition system needed to be adapted to the needs of seismology as far as timing accuracy and sampling rate were concerned. The complete permanently recording system consists of the ring laser (one component of rotation around the vertical axis), two tiltmeters oriented N–S and E–W, as well as temperature and atmospheric pressure sensors. About 300 m away from the ring laser instrument a seismic broad-band station (station name WET, Lat = 49.15°, Lon = 12.88°, German Regional Seismic Network) is recording permanently three orthogonal ground velocity components. The STS-2 broad-band sensor records at 20 Hz sampling rate and has a flat response from 8.33 mHz ($T = 120$ s) to 50 Hz. All broad-band seismograms were deconvolved with the instrument response function to a uniform seismometer. One of the attractive features of optical sensors is the uniform transfer function through the mass-less recording system. Thus, no instrument correction is necessary for the rotational measurements. To enable sample-by-sample comparison (e.g. using cross-correlation techniques) the rotational signal—originally sampled at 4 Hz—was resampled to the 20 Hz sampling rate of the translational recordings. The horizontal seismograms were rotated in a local radial-transverse system and the transverse component differentiated in time to obtain transverse acceleration (see below). Given the frequency range (and thus the spatial wavelengths) considered in this data analysis (∼0.007–1.0 Hz) the two instruments (ring laser and broad-band seismometer) are treated as collocated. This may lead to non-negligible effects at the high-frequency end of this interval for local events. From the permanent observations in 2003 and 2004, a total of 18 events were chosen for this analysis. The choice was primarily based on the signal-to-noise (S/N) ratio of the ring laser observations and the desire to cover a wide enough magnitude and distance range. Information on these events is summarized in Table 1, and their magnitude–distance distribution visualized in Fig. 2 (top). The events cover a distance range of 370–12 700 km and magnitudes from M5.0 (local event in Germany) to M9.0 (the Great Andaman earthquake).

OBSERVATIONS AND PROCESSING

In this section we compare translational and rotational measurements with the primary goal to verify whether the ring laser produces measurements that are consistent with what we know on elastic wave propagation. In order to do this, we exploit a very simple relationship between transverse acceleration and rotation rate that is obtained assuming plane wave propagation in horizontal direction with transverse polarization. As used earlier in a similar context (e.g. Pancha *et al.* 2000; Igel *et al.* 2005), the transverse acceleration a_T is equal to the vertical component of rotation rate Ω_z multiplied by twice the local (apparent) horizontal phase velocity c: $a_T(x, t) = 2c\Omega_z(x, t)$. In other words, under the plane wave assumption, transverse acceleration and rotation rate should have the

COLOUR FIG.

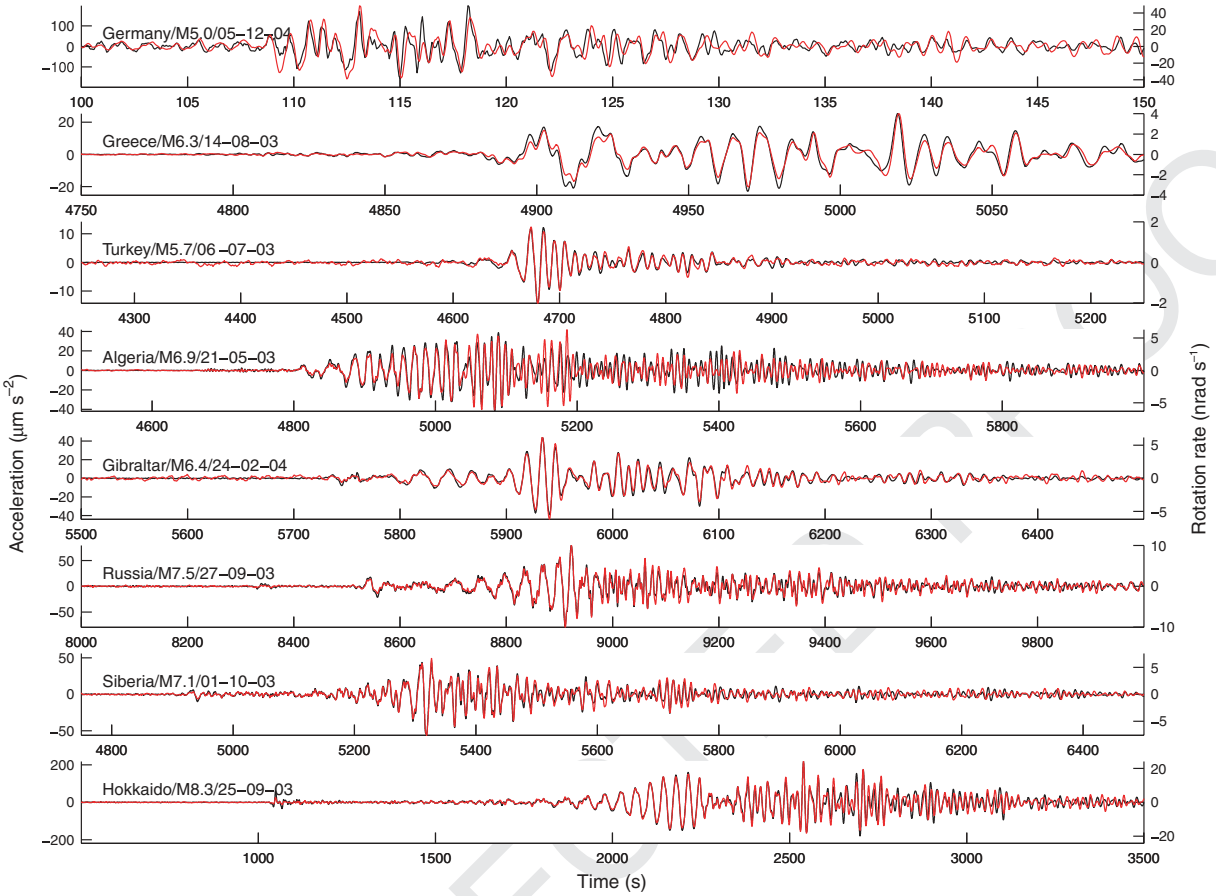

Figure 3. Superposition of transverse acceleration (black, left axis) and rotation rate (red, right axis) for several events listed in Table 1. The translations were corrected for the instrument response.

same waveform and their amplitudes should scale proportionally to phase velocity depending on wave type (e.g. shear waves, Love waves) and propagation direction. In Table 1, the S/N ratios of all events for both transverse acceleration and rotation rate are given. The ratios were determined by calculating the ratio of covariances in a 1000-sample (50 s) time window prior to the first break and around the peak signal. The results in Table 1 indicate that the S/N ratio of the translations is approximately 2–3 orders of magnitude larger. Nevertheless, in some cases the waveform fit (measured by the zero-lag normalized cross-correlation coefficient, see discussion below) between transverse accelerations and rotation rate is excellent (e.g. Irian Jaya events) despite the fact that the S/N ratios are low.

MAGNITUDE SCALES AND ROTATIONS

As a first step we investigate whether the peak rotation rates observed are consistent with those expected from the definition of the surface wave magnitude M_S (e.g. Shearer 1999)

$$M_S = \log_{10}\frac{A}{T} + 1.66\log_{10} D + 3.3. \qquad (2)$$

A is the surface wave amplitude (in micrometres), T is period (in s), and D is the epicentral distance (in degrees). Using the relationship between displacement and rotation rate we obtain the rotation rate as a function of surface wave amplitude

$$\Omega_z = 2\frac{\pi^2}{cT^2}A(M_S, D) = 2\frac{\pi^2}{cT}10^{M_S - 1.66\log_{10} D - 9.3}, \qquad (3)$$

in rad s^{-1} (note that the inconsistency in dimensions on the right-hand side comes from the non-dimensional definition of the magnitude scale). Eq. (3) provides us with the distance- and period-dependent rotation rate to be expected in the domain of applicability of the surface wave magnitude scale (20°–160°).

To compare our observations with this prediction we filter the rotation rate of all events in the M_S distance range in a narrow band with central period $T = 30$ s and extract the peak rotation rate as a function of distance. The required Love wave phase velocity c in eq. (3) was chosen as 4200 m s^{-1} derived from the theoretical Love wave dispersion curve for a spherically symmetric earth model based on ak135 (Kennett *et al.* 1995). The results are shown in Fig. 2, bottom. Peak rotation rates are compared with the theoretical predictions for M6–M9 earthquakes at $T = 30$ s on a semi-log scale. Given the relatively large uncertainties of single station magnitude estimations, the observations match the theoretical predictions quite well. Effects such as directivity can be used as an explanation for the observed scatter. In addition, the rotation rate for the M9 Great Andaman earthquake is smaller than expected. This is likely to be due to a finite-source effect well documented also for the magnitude estimates based on translations. Nevertheless, the results indicate a fair consistency of rotation rate amplitudes over a distance range of several thousands of kilometres and two orders of magnitude in amplitude.

COLOUR FIG.

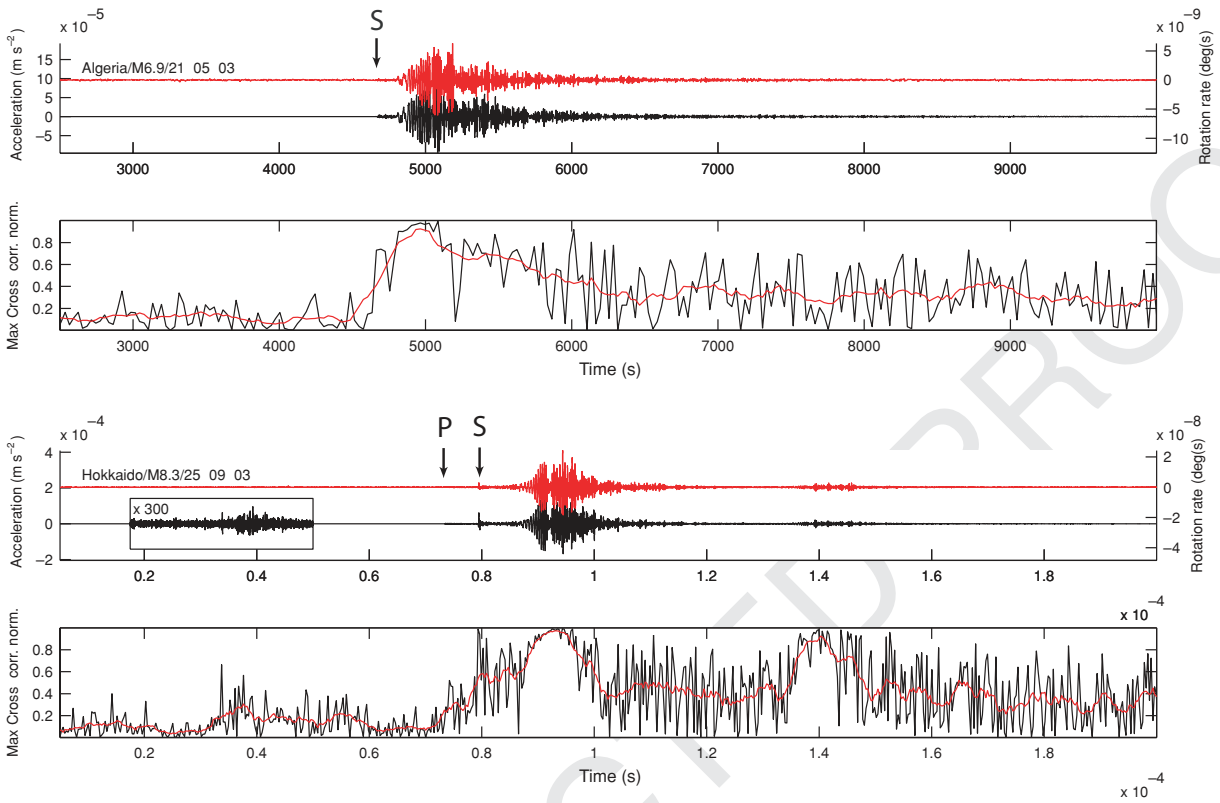

Figure 4. Rotation rate (red, right axis) and transverse acceleration (black, left axis) and maximum normalized (zero-lag) cross-correlation as a function of time in a 20 s sliding time window (black line) and a smoothed average (red line). Top: Algeria event, 2004 February 24, M6.4. Bottom: Hokkaido event, 2003 September 25, M8.3. The inlet shows arrivals from another earthquake visible in the transverse accelerations after magnification by a factor of 300.

COLLOCATED MEASUREMENTS OF TRANSLATIONS AND ROTATIONS

As indicated in the introduction to this section—according to the relation between transverse acceleration and rotation rate—we expect the waveforms to be identical provided that the assumption of plane wave propagation is fulfilled. In Fig. 3 we show transverse acceleration (black) and rotation rate (red), both unfiltered, for a selection of earthquakes listed in Table 1 covering most of the magnitude and distance range. The time-series are shown with the corresponding axis dimensions (m s^{-2} and rad s^{-1}) and the amplitudes are scaled such that the maxima have equal amplitude in the graph. Note that the length of the time windows vary, indicating the different dominant frequencies for local and global events.

Nevertheless, there is striking visual waveform similarity between transverse acceleration and rotation rate for all recorded events. This similarity is not limited to the most dominant Love wave signals but the fit continues long after the fundamental mode surface waves (e.g. Greece event at $t \approx 4900$ s; Turkey event at $t \approx 4680$ s; Gibraltar at $t \approx 5900$ s; Hokkaido at $t \approx 2000$ s) have passed. This is a strong indication that—at least as far as waveforms are concerned—the plane wave assumption is approximately fulfilled even for high frequencies (close to 1 Hz) observed for the local M5 event in Germany. These observations also seem to suggest that the ring laser instrument is indeed recording rotational motions with a uniform response over a wide frequency range. For some of the events (e.g. Algeria, Russia, Hokkaido) the waveform fit deteriorates towards the end of the time-series. This may indicate that scattered body waves (*SH*-type) or higher-mode Love waves arrive from different azimuths and that the transverse direction chosen according to the theoretical backazimuth (BAZ) is no longer appropriate. In addition, the assumption of independent (non-dispersive) horizontal wave propagation may not hold. These waveform differences may contain information on the amount of scattering, the non-planarity of wave fronts, and the direction of propagation (see below). Understanding of these issues would require comparison with synthetic modelling of wave propagation through 3-D structures.

CROSS-CORRELATION OF TRANSLATIONS AND ROTATIONS

Cross-correlation techniques allow the quantification of the similarity of two discrete functions. We quantify the time-dependent similarity between rotation rate and transverse acceleration by sliding a time window of appropriate length (longer than one dominant period) along the time-series and calculate the zero-lag normalized cross-correlation coefficient that is defined between 0 (no similarity) and 1 (perfect match). This procedure is illustrated for two events (Algeria and Hokkaido) in Fig. 4. In both events the coefficients before the first breaks are around 0.2–0.3 indicating the lack of any systematic waveform similarity. For the Algeria event (Fig. 4, top) the coefficient jumps to values above 0.7 with the arrival of the direct shear wave (at approx. 4600 s) and—after shortly dropping below 0.4—increases to values close to one in the time window containing Love waves (after approx. 4800 s), confirming the visual impression of Fig. 3. One of the most striking features universally seen for all event data is the continuous increased correlation long after the main phases have passed. This indicates that (scattered)

COLOUR FIG.

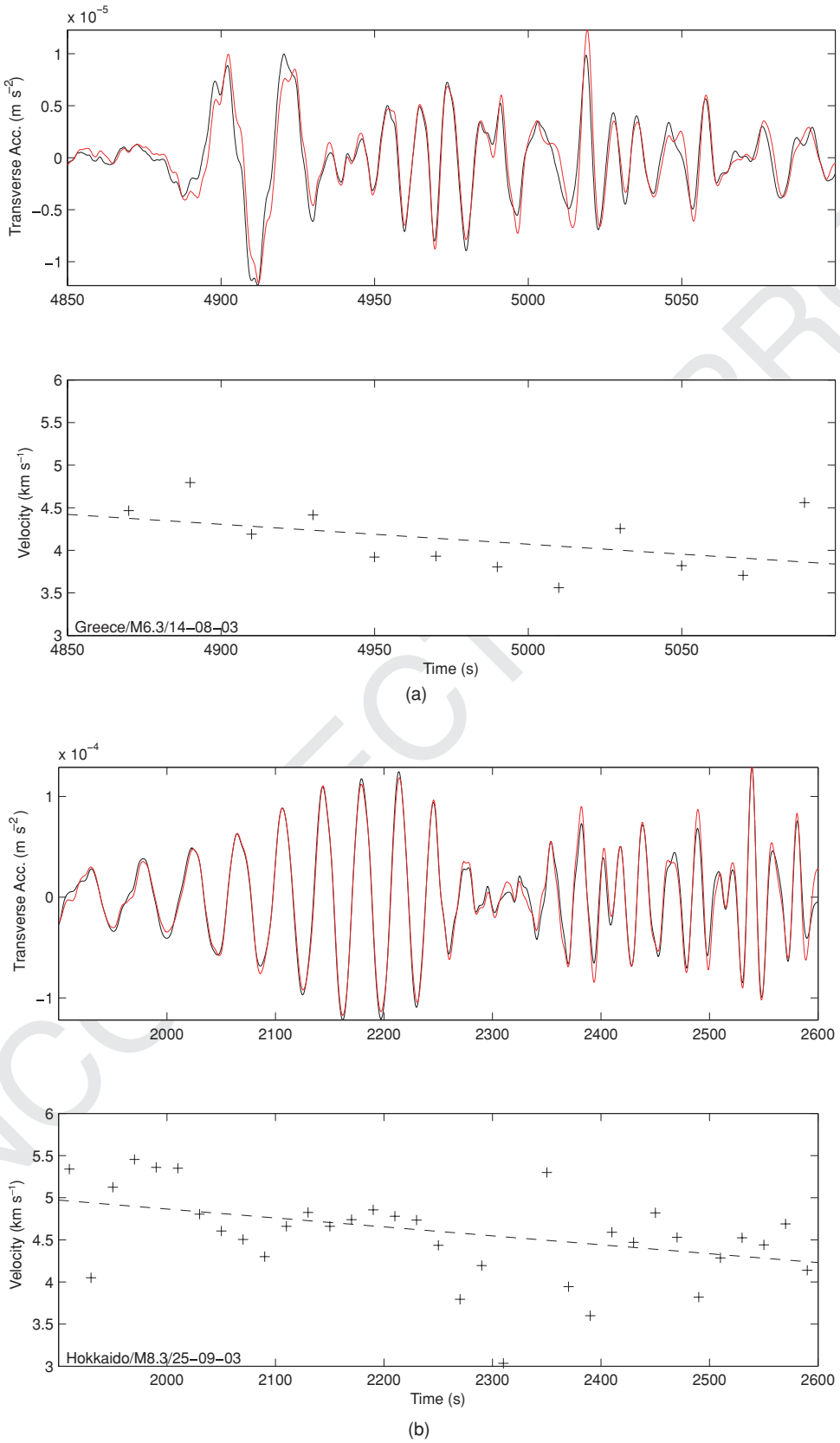

Figure 5. (a) Superposition of transverse acceleration (black, left axis) and rotation rate (red, scaled to match in amplitude) and determination of phase velocities as a function of time in a 20 s sliding window and a best-fitting line. Event in Greece, M6.3, 2003 August 14. (b) Same as Fig. 5(a). Event in Hokkaido, M8.3, 2003 September 26. (c) Same as Fig. 5(a). Event in Russia, M7.5, 2003 September 27. (d) Same as Fig. 5(a). Event in Siberia, M7.1, 2003 October 1.

COLOUR FIG.

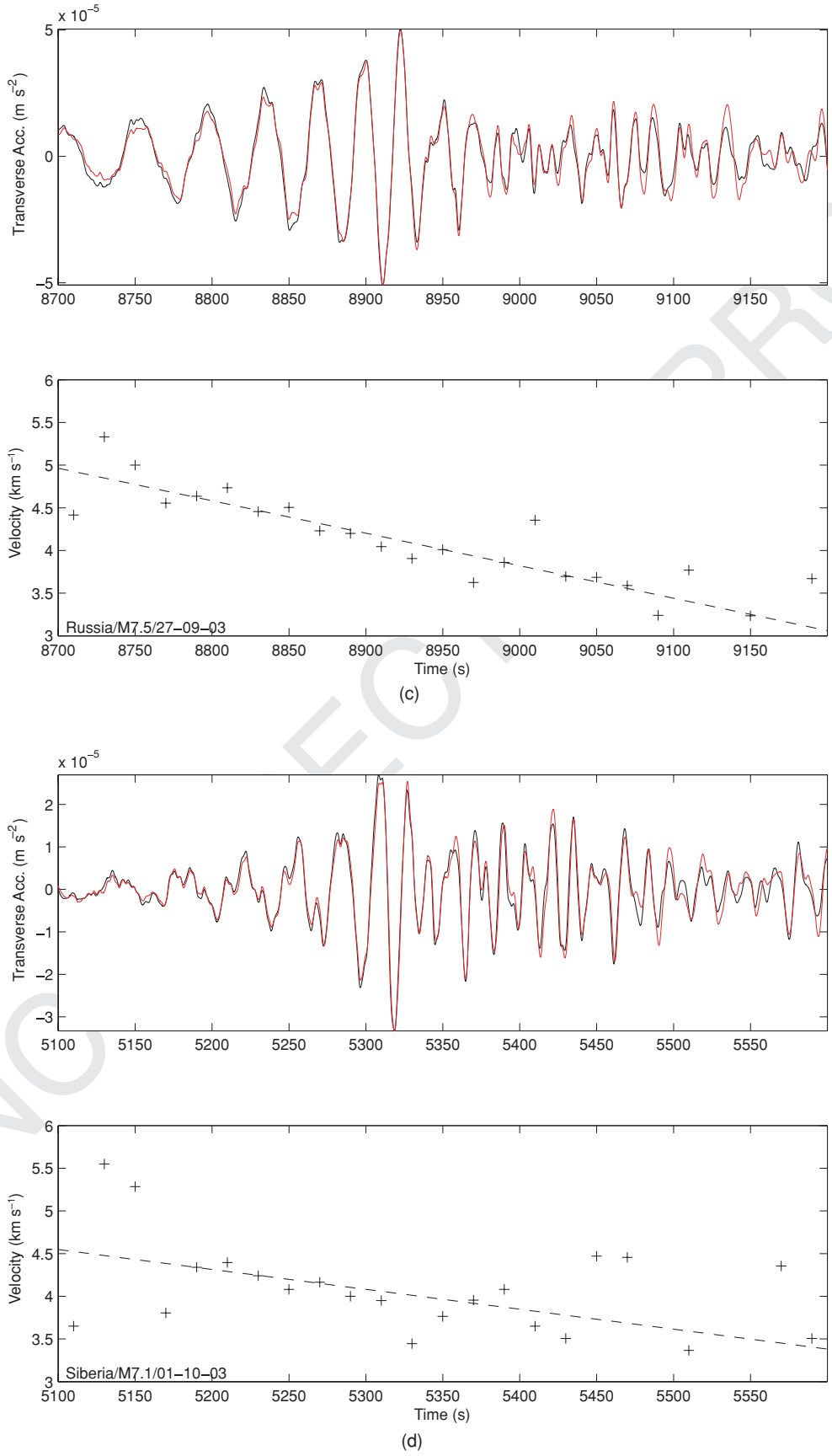

Figure 5. (*Continued.*)

COLOUR FIG.

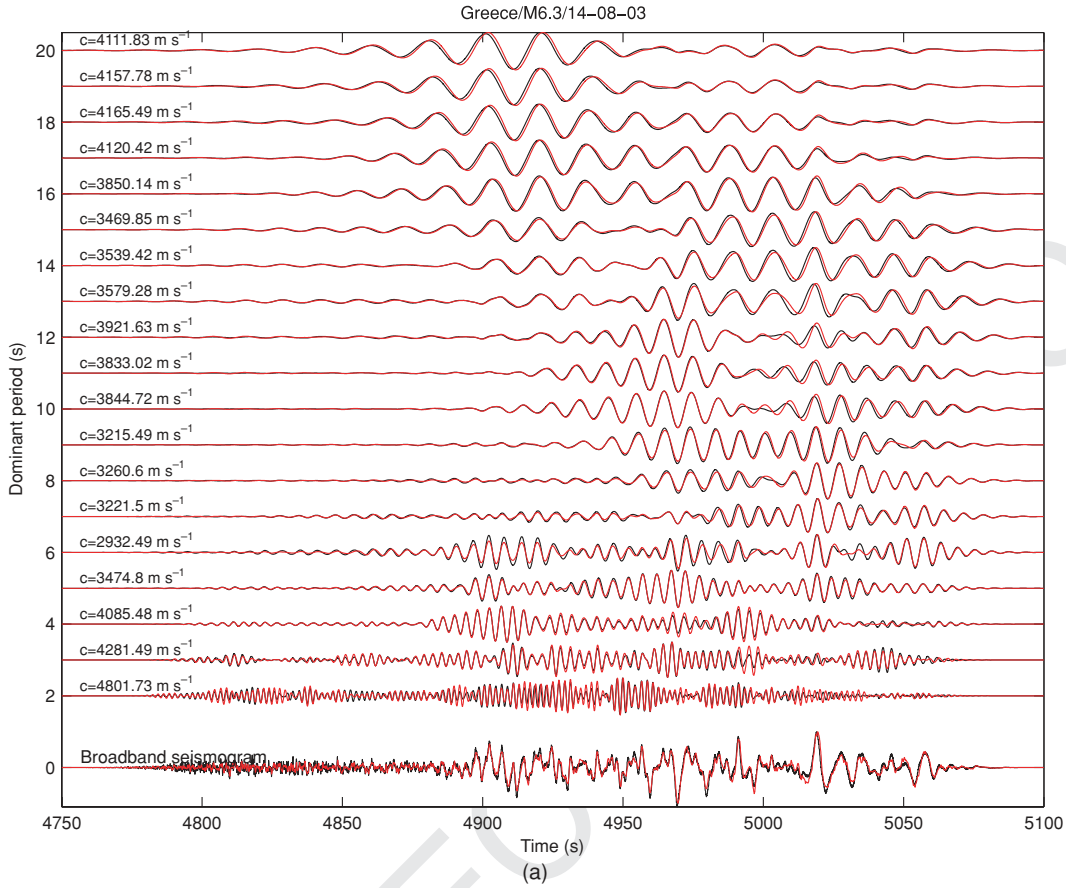

Figure 6. (a) Superposition of transverse acceleration (black) and rotation rate (red) and determination of phase velocities as a function of dominant period after narrow-band filtering (see text for details). The phase velocities given for each trace pair were determined by dividing the peak transverse acceleration by the peak rotation rate. Event in Greece, M6.3, 2003 August 14. (b) Superposition of transverse acceleration (black) and rotation rate (red) and determination of phase velocities as a function of dominant period after narrow-band filtering (see text for details). The phase velocities given for each trace pair were determined by dividing the peak transverse acceleration by the peak rotation rate. Event in Hokkaido, M8.3, 2003 September 25.

SH-type wave motion continues to arrive at the recording site leading to significant correlation even though the S/N ratio of the ring laser recording has dropped below unity.

To further illustrate the detective power of the cross-correlation technique a time window of almost 6 hr containing the M8.3 event in Hokkaido is shown in Fig. 4 (bottom). As in the previous case the background coefficient is around 0.2–0.3. There is a sudden increase in correlation at around $t = 3400$ s, that could only be explained after blowing up the transverse acceleration indicating a seismic event just above noise level (see inlet magnified by a factor of 300). This following systematic increase in (average) correlation above the noise level is caused by the event identified as the M5.7 earthquake that happened the same day at the Mid-Atlantic Ridge (Lat 35.35, Lon −35.86 at 18:43:06, 2003 September 25). The coefficient increases again systematically with the onset of the *P* waves at $t = 7500$ s. This is somewhat surprising, as—assuming a spherically symmetric earth model—there should be no rotational energy observable before the onset of the direct *SH* wave. This indicates that *P*–*SH* scattering may be responsible for the increase in correlation in the *P* coda. This is discussed in more detail below.

The coefficient increases to values close to unity with the onset of the direct shear wave and the Love waves. It remains close to unity for most of the time window containing the fundamental and higher-mode Love waves and remains at a high level (above 0.6) until the signals from the first aftershock (M7.4, at 21:08:00 2003 September 25) arrive at around $t = 13\,500$ s, again increasing the level again close to perfect fit. The results shown in Fig. 4 (similar behaviour is observed for the other events) confirm in a quantitative way the expected phase relation between transverse acceleration and rotation rate despite the simplified assumptions of plane-horizontal non-dispersive wave propagation with transverse polarization. The zero-lag normalized cross-correlation coefficient in a 50 s time window around the peak value is given for all events in Table 1. The values reach 0.997 (Turkey, Hokkaido) indicating an almost perfect waveform match as seen visually in the figures discussed above.

HORIZONTAL PHASE VELOCITIES AND FREQUENCY DEPENDENCE

The observations discussed above demonstrate the *phase* consistency of the collocated measurements. The consistency of the rotation-rate *amplitudes* can be investigated by exploiting the expected proportionality between transverse acceleration and rotation rate being equal to twice the horizontal phase velocity. Assuming correct transverse accelerations, the rotational amplitudes are consistent if the resulting phase velocities are compatible with theoretical predictions for earth models within some bounds. Clearly, we do not expect phase velocities to be uniform for the whole seismogram. The phase velocity of *SH*-type body waves will depend on the

COLOUR FIG.

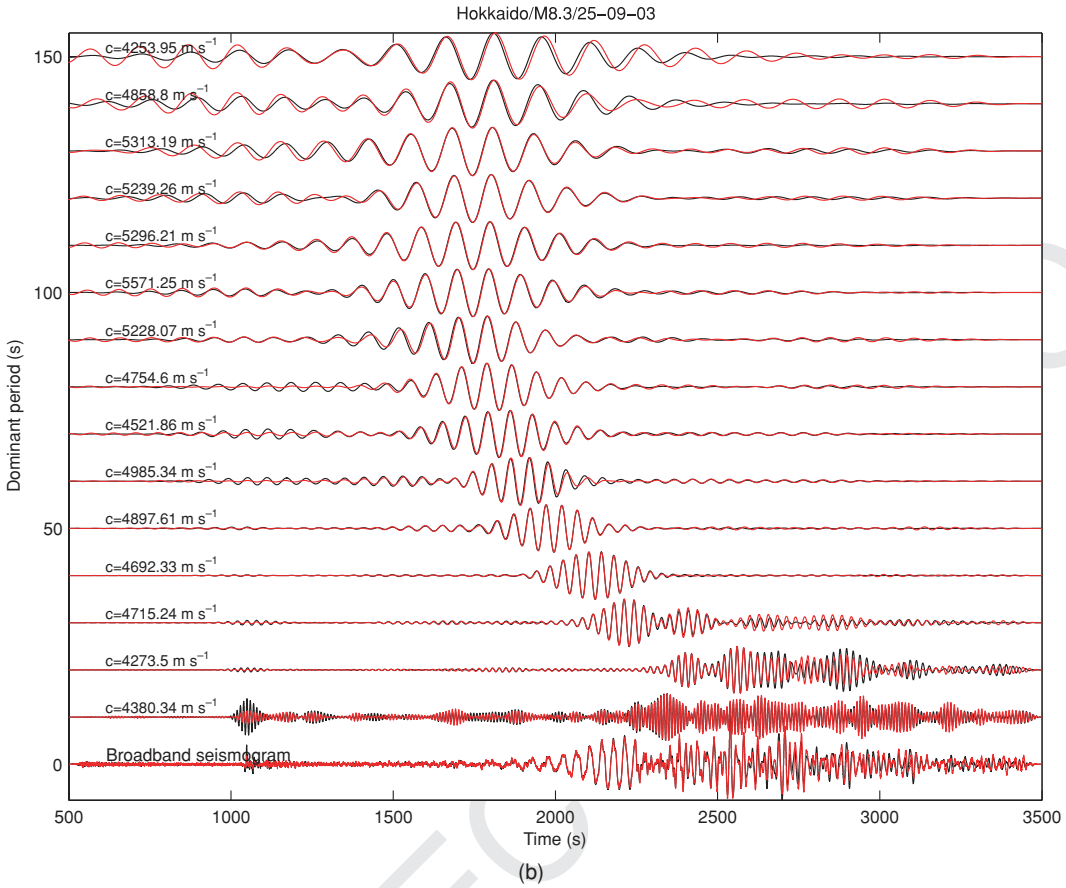

Figure 6. (*Continued.*)

angle of incidence (it will thus be an apparent phase velocity) and we expect that the dispersive behaviour of Love waves will lead to the variation of horizontal phase velocity with frequency (and thus with time along the time-series).

In sliding time windows of length $T = 20$ s covering the Love wave arrivals, the horizontal phase velocity is estimated by finding the optimal scaling (least squares) between rotation-rate and acceleration. The phase velocity thus obtained is plotted as a function of time together with the time signals. A line is fit to the estimated phase velocities using least squares. This processing is shown for four events in Figs 5(a)–(d). In all four events the dominant period is visually decreasing with time. The estimated phase velocities and the average behaviour show decreasing phase velocities with time (and increasing frequency) as is expected for dispersive Love waves. For a spherically symmetric earth model Love wave phase velocities (e.g. Kennett 2002) would be in the range of 3800 m s^{-1} (at $T = 10$ s) to 4500 m s^{-1} (at $T = 50$ s). This is indeed the range of velocities we observe for the events chosen in Fig. 5. It is obvious, that the phase velocity estimates could also be carried out in the frequency domain by calculating amplitude-spectral ratios in the relevant frequency band and by choosing the appropriate time windows. The discussion here remains semi-quantitative. A detailed analysis of the possibility to derive Love wave dispersion from collocated measurements goes beyond the scope of this paper and is reported in a separate study (Suryanto *et al.* 2006b). Nevertheless, the estimate of phase velocities, a wavefield property that is otherwise only accessible through array measurements or additional strain measurements (e.g. Mikumo & Aki 1964), is an attractive feature of the four-component measurements discussed here. Estimates of horizontal phase velocities in a 50 s time window containing the peak signal are summarized for all events in Table 1. The results suggest that distant events (e.g. Hokkaido, Siberia, etc.) are characterized by higher phase velocities than close events (e.g. Germany, Greece), indicating the lower frequencies of distant events and consequently faster Love wave phase velocities.

To further illustrate the frequency-dependent performance of the rotational sensor compared with the broad-band seismometer we superimpose transverse acceleration and rotation rate after filtering with a narrow bandpass (zero-phase Butterworth with corner frequencies $0.9 \times 1/T$ Hz and $1.1 \times 1/T$ Hz, where T is the period in seconds). In Fig. 6, two examples (a regional event, Greece, and a distant event, Hokkaido) are compared as a function of dominant period and superimposed by scaling with the appropriate phase velocity (given at the top of each trace pair) obtained by dividing the peak amplitudes. For the regional event (Greece), the waveform fit is excellent for periods between $T = 3$–20 s not only for the Love wave part but also for the earlier body wave arrivals. For the case of the distant event (Hokkaido), the waveforms match well for $T = 20$–150 s further confirming the consistent behaviour of the rotational sensor for long periods. The estimated phase velocities show—as above as a function of time—the trend to higher phase velocities as the frequency decreases. It is important to note that the phase match for lower frequencies was only possible after correcting the broad-band seismograms for their instrument response. Without this processing step the fundamental Love wave groups would show phase differences of tens of seconds (for periods longer than 100 s) and the

COLOUR FIG.

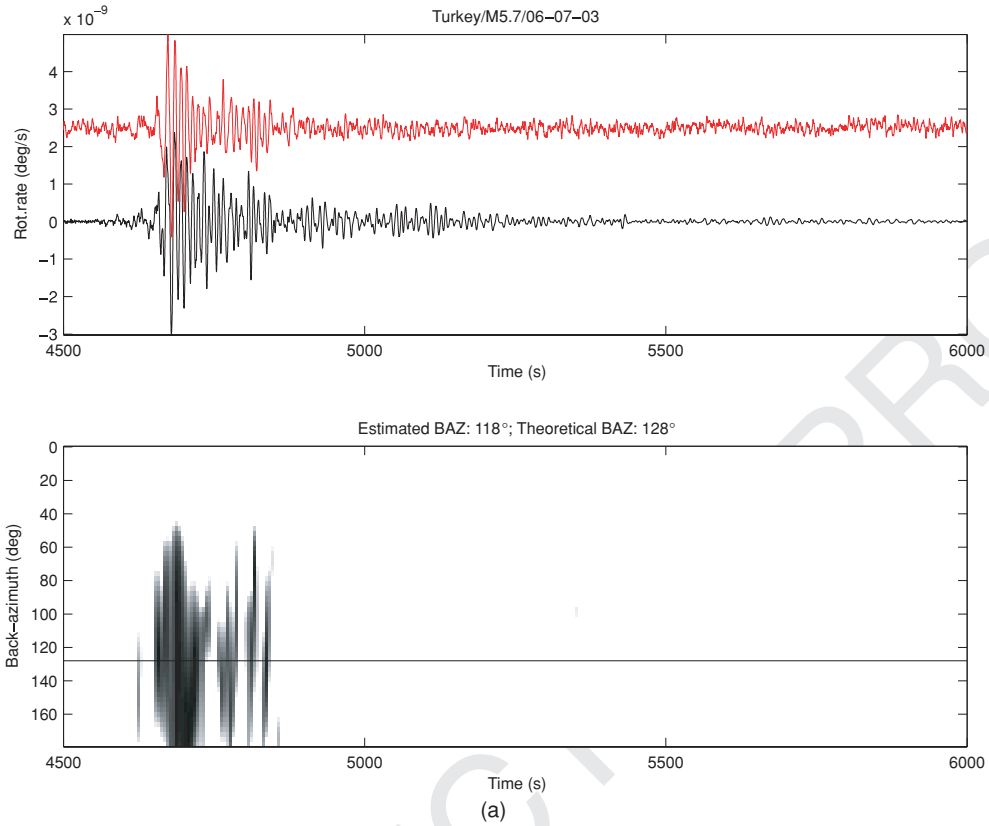

Figure 7. (a) Top: Rotation rate and transverse acceleration (scaled to rotation rate) for the Turkey event, M5.7, 2003 July 6. Bottom: Zero-lag normalized correlation coefficient in a 20 s sliding time window between rotation rate and transverse acceleration, varying the unknown transverse direction from 0° to 180° (defined between 0.9-white and 1.0-black). The theoretical backazimuth is indicated by a horizontal line (see text for details). (b) Top: Rotation rate and transverse acceleration (scaled to rotation rate) for the Siberia event, M7.1, 2003 October 1. Bottom: Zero-lag normalized correlation coefficient in a 20 s sliding time window between rotation rate and 'transverse' acceleration, varying the unknown transverse direction from 0° to 180° (defined between 0.9-white and 1.0-black). The theoretical backazimuth is indicated by a horizontal line (see text for details).

estimated phase velocities would diverge to values much too small. To some extent this can be considered an independent evaluation of the quality of the instrument response correction process.

PROPAGATION DIRECTION—BACKAZIMUTH

The estimation of the local horizontal phase velocity demonstrates the potential to reliably estimate wavefield properties otherwise only accessible through array measurements (or using strain in an analogous manner). Another such wavefield property is the propagation direction of *SH*-type motions. So far, we have pre-processed the data in the sense that they were rotated into transverse and radial components according to the theoretical BAZ derived from epicentral and station coordinates. In the following we treat the BAZ as unknown and seek propagation directions that maximize the correlation coefficient in sliding windows of appropriate length along the whole seismogram. This is the extension of the type of analysis shown in Fig. 4 to all propagation directions.

In Fig. 7 two events (Turkey and Siberia) are processed in this way using a sliding window length of 10 s and an azimuthal range of 0°–180° from North. Below the rotation rate (red) and the original transverse component of acceleration (black, converted to rotation rate using a phase velocity of 4000 m s^{-1}) the zero-lag correlation coefficient as a function of time and BAZ is shown in the same time window as the seismograms. As expected, the maxima of the correlations (black) are found in the window containing the Love wave arrivals. Before and after there is considerable scatter which may indicate *SH*-type energy arriving with different BAZs. When the correlation coefficients are summed up over times slices with sufficient peak correlation (e.g. 0.9), we can estimate the BAZ by finding the maximum of the distribution of correlation coefficients and the associated BAZ. The differences between theoretical and estimated values (10° for the Turkey event, 5° for the Siberia event) are relatively small. It remains to be seen how stable such estimates are, and whether the discrepancies may indicate the influence of 3-D structure on the propagation direction or the non-planarity of the wave fronts.

ROTATIONAL SIGNALS IN THE *P* CODA

Finally, as indicated above, it was surprising to see a clear increase in correlation between transverse acceleration and rotation rate coinciding with the onset of the direct *P* wave. Theoretically, in isotropic media the rotation sensor is insensitive to *P* waves and signals are expected only from *SH*-type motions. However, at the Earth's surface *P* and Rayleigh waves lead to tilting (also rocking, rolling, or rotational motions around the transverse axes) that pollutes the ring laser measurements through changes of the surface normal with respect

COLOUR FIG.

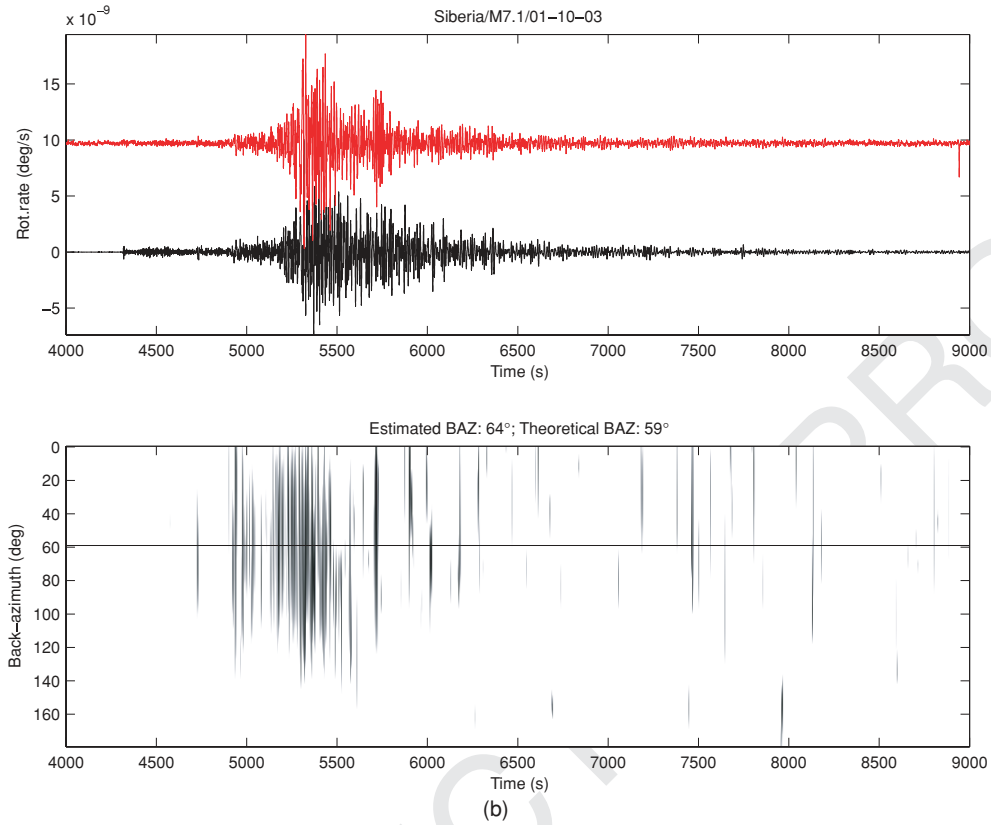

Figure 7. (*Continued.*)

to the Earth's rotation axis. The tilt signal can be estimated roughly from the vertical component of motion and the corresponding effect on rotation through eq. (1) (there are tiltmeters installed on the G-ring, however—as is well known—they are sensitive to transverse acceleration in the frequency band investigated here. This is studied in more detail elsewhere). The estimated contribution is so small in comparison with the observed noise level that it can be ruled out as cause for the significant increase in correlation. The other explanation for the observed increase is *P–SH* converted energy close to the receiver. This phenomenon would require 3-D scattering as in layered media *P* would only scatter into SV type motions that the ring laser would not detect.

In order to quantify and document this effect more clearly we high-pass filter both signals (transverse acceleration and rotation rate) and calculate the zero-lag cross-correlation coefficient as a function of cut-off period as we expect this effect to be most pronounced in the frequency band of the directly arriving *P*-energy (around 1 Hz). Two examples (Gibraltar and Hokkaido events) are shown in Fig. 8 using sliding windows of twice the cut-off period. In both events there is a sharp increase in correlation with and just following the direct *P* wave (clearly visible in the trace showing the vertical acceleration). This correlation smears out and becomes less pronounced with increasing period, while the corresponding correlation of *SH*-type signals and Love waves increases with period (e.g. Fig. 8a: *P*-arrival for Gibraltar event at $t = 5530$ s compared to *S* arrival at $t = 5740$ s; Fig. 8(b): *P*-arrival at $t = 7400$ s; *S*-arrival at $t = 7950$ s). These observations may provide a means to estimate near-receiver *P–SH* scattering in a quantitative way thereby separating out *SH* motions from the scattering field. To study this in more detail will require observations at different sites and appropriate simulation tools for 3-D media at high frequencies.

DISCUSSION AND CONCLUSIONS

For decades the direct observation of rotational ground motions was difficult due to the lack of appropriate rotation sensor that were able to record earthquake-induced motions at high enough sensitivity. Despite the lack of observations—particularly in the fields of earthquake engineering and strong ground motion—the problem was addressed on a more theoretical level (or through conversion of translations) with the aim of finding the role of rotational motions in earthquake-induced damage of buildings (Castellani & Boffi 1986, 1989; Castellani & Zembaty 1996; Li *et al.* 2001, 2002; Lee & Trifunac 1985, 1987; Niazi 1986; Oliveira & Bolt 1989). In seismology, rotations are discussed particularly in connection with seismic instrumentation, as it is well known that rotational ground motions are polluting inertial observations of translational ground motions which is the reason why it is so difficult to derive displacement histories from velocity or acceleration sensors. There are very few studies in which rotational motions were observed with low-sensitivity sensors (e.g. Nigbor 1994; Takeo & Ito 1998), and some through seismic array measurements (Singh *et al.* 1997; Huang 2003). There is only one study in which array measurements were compared with direct measurements of rotations (Suryanto *et al.* 2006a).

In the past decade ring laser technology was applied in Earth sciences and geodesy primarily to study changes in the Earth's rotation at very high precision. The observation of earthquake-induced rotational motions came as a by-product (e.g. Stedman *et al.* 1995) but opened the possibility for the first time to analyse collocated

Q3

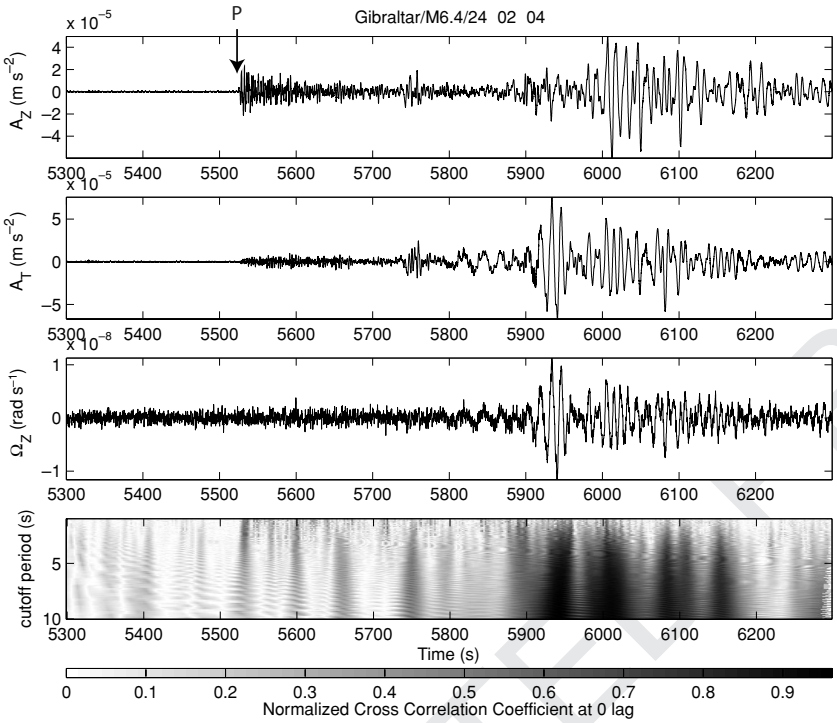

(a)

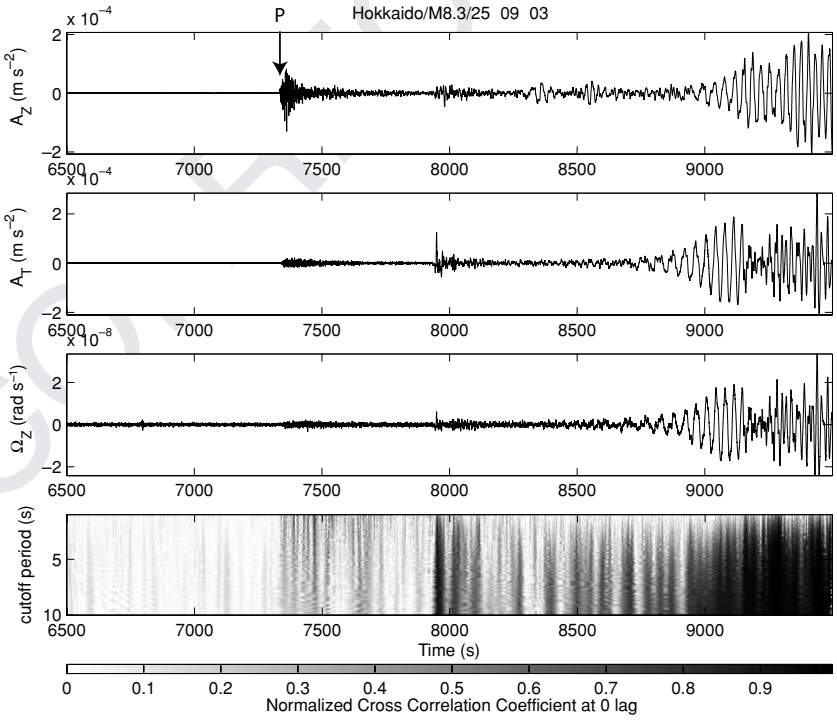

(b)

Figure 8. (a) Top: Vertical acceleration, transverse acceleration, and rotation rate for the Gibraltar event, M6.4, 2004 February 24. Bottom: Zero-lag normalized cross-correlation coefficient between transverse acceleration and rotation rate in a sliding time window twice as long as the high-pass cut-off period applied before correlating (left axis). (b) Top: Vertical acceleration, transverse acceleration, and rotation rate for the Hokkaido event, M8.3, 2003 September 25. Bottom: Zero-lag normalized cross-correlation coefficient between transverse acceleration and rotation rate in a sliding time window twice as long as the high-pass cut-off period applied before correlating (left axis).

observations of rotations and translations in a seismological context. The first studies focused on the understanding of the various contributions to the ring laser signal (McLeod *et al.* 1998; Pancha *et al.* 2000) and the analysis of single events in the context of plane wave theory as shown above. However, these initial studies did not show full consistency of the rotational ground motions with translations and comparison was done in a very narrow frequency band. Nevertheless these pilot studies indicated that the ring laser is capable of observing the small amplitudes resulting from distant earthquakes. After the installation of the high-sensitivity ring laser (G-ring) at the Fundamentalstation in Wettzell, SE-Germany, the goal was to systematically investigate earthquake-induced rotational motions. At the onset of this study it was not clear whether the measurements in the frequency domain relevant for seismology are strongly influenced by local structure and/or the specific instrumental installation (e.g. cave effects), as is well known for strain measurements (e.g. Gomberg & Agnew 1996). In the light of this, the main goal of this study was to test the fitness of ring laser technology for seismological purposes. While the observations with the G-Ring were investigated, a purpose-built ring laser system (named Geosensor) was developed specifically for seismology with similar sensitivity (Schreiber *et al.* 2005). Two of those instruments are now operational, one at the Piñon Flat Observatory, California, one in a building of Christchurch University, New Zealand.

The results shown in this study show a remarkable consistency between rotational ground motions around a vertical axis and transverse acceleration primarily quantified by the cross-correlation coefficient that is calculated in sliding time windows along the observations. This correlation seems to be stable for periods of 1 s (local events, body waves) up to long-period signals (150 s, Love waves) and it is likely that this can be extended to lower frequencies particularly if the sensitivity increases. In addition, the phase velocities estimated by taking the ratio of transverse acceleration and rotation rate, are compatible with the expected velocities assuming plane transverse wave propagation, confirming recent results that were limited to the analysis of a single distant event (Igel *et al.* 2005; Cochard *et al.* 2006) with support through synthetic modelling. This implies that the multi-component observations allow the estimate of wavefield properties (e.g. phase velocities, propagation direction) that otherwise are only accessible with high accuracy through array (or to some extent additional strain) measurements. The accuracy of the Love wave dispersion estimates is being investigated and compared to array-derived values (Suryanto *et al.* 2006b).

In summary, we believe, it is fair to say that seismology now has the 'suitable instrument for making such measurements' (i.e. rotations), that Aki & Richards (2002) were waiting for. However, it remains to be seen whether the technology can be further adapted to the specific needs of seismology particularly in terms of portability, or whether other types of sensors (e.g. solid-state sensors, fibre-optic gyros) can be made accurate enough to fill the gap between high- and low-sensitivity requirements for seismology. Nevertheless, the new observations of rotations not only opens new possibilities in processing and data analysis, but also pose several questions that need to be addressed in the future:

(1) How can we explain the observations of rotations in the *P* coda?

(2) Do observations at other observing sites show similar consistency and overall behaviour?

(3) What are the consequences of non-planar wave fronts (e.g. Wielandt, 1993) and the inclusion of dispersive effects?

(4) What is the influence of seismic anisotropy on rotational measurements, to name but a few.

To answer these questions, observations at different locations combined with sophisticated modelling of wave propagation will be necessary.

ACKNOWLEDGMENTS

This work was supported by the German Ministry of Research and Education (BMBF-Geotechnologien) and German Research Foundation. AF was supported by the German Academic Exchange Service (IQN-Georisk). We acknowledge the contributions of the Bundesamt für Kartographie und Geodäsie (BKG) towards the installation and operation of the 'G' ring laser at the geodetic observatory Wettzell. We are grateful to Richard Bennett who processed the broad-band data. We thank Wolfgang Friederich for providing the code to calculate Love wave dispersion curves. Thanks to Jean Virieux and two anonymous reviewers for comments.

REFERENCES

Aki, K. & Richards, P.G., 2002. *Quantitative Seismology,* 2nd edn, University Science Books,.

Bouchon, M. & Aki, K., 1982. Strain, tilt, and rotation associated with strong ground motion in the vicinity of earthquake faults, *Bull. seism. Soc. Am.,* **72,** 1717–1738.

Castellani, A. & Boffi, G., 1989. On the rotational components of seismic motions, *Earth. Eng. Struct. Dyn.,* **18,** 785–797.

Castellani, A. & Boffi, G., 1986. Rotational components of the surface ground motion during an earthquake, *Earth. Eng. Struct. Dyn.,* **14,** 751–767.

Castellani, A. & Zembaty, Z., 1996. Comparison between earthquake rotation spectra by different experimental sources, *Engineering Structures,* **18,** 597–603.

Cochard, A. *et al.*, 2006. Rotational motions in seismology: theory, observations, simulation, in '*Earthquake Source Asymmetry, Structural Media and Rotation Effects*' eds Teisseyre*et al.*, Springer Verlag.

Farrell, W.E., 1969. A gyroscopic seismometer: measurements during the Borrego Earthquake, *Bull. seism. Soc. Am.,* **59,** 1239–1245.

Gomberg, J. & Agnew, J., 1996. The accuracy of seismic estimates of dynamic strains: an evaluation using strainmeter and seismometer data from Pinon Flat Observatory, California, *Bull. seism. Soc. Am.,* **86,** 212–220.

Graizer, V.M., 2005. Effect of tilt on strong motion data processing, *Soil Dyn. Earthq. Eng.,* **25,** 197–204.

Graizer, V.M., 2006. Equation of pendulum motion including rotations and its implications to the strong-ground motion, in Earthquake Source Asymmetry, Structural Media and Rotation Effects, 471–491.

Huang, B.-S., 2003. Ground rotational motions of the 1999 Chi-Chi, Taiwan earthquake as inferred from dense array observations, *Geophys. Res. Lett.,* **30,** doi:10.1029/2002GL015157.

Igel, H., Schreiber, K.U., Flaws, A., Schuberth, B., Velikoseltsev, A. & Cochard, A., 2005. Rotational motions induced by the M8.1 Tokachi-oki earthquake, September 25, 2003, *Geophys. Res. Lett.,* **32,** L08309, doi:10.1029/2004GL022336.

Kennett, B.L.N., 2002. The Seismic Wavefield, Volume II: Interpretation of Seismograms on Regional and Global Scales, Cambridge University Press.

Kennett, B.L.N. Engdahl, E.R. & Buland, R., 1995. Constraints on seismic velocities in the Earth from travel times, *Geophys. J. Int.,* **122,** 108–124.

Lee, V.W. & Trifunac, M.D., 1985. Torsional accelerograms, *Soil. Dyn. Earthq. Eng.,* **4,** 132–142.

Lee, V.W. & Trifunac, M.D., 1987. Rocking strong earthquake accelerations, *Soil. Dyn. Earthq. Eng.,* **6,** 75–89.

Lefevre, H., 1993. *The fibre optic gyroscope*, Artech, Norwood.

Li, H.-N., Sun, L.-Y. & Wang, S.-Y., 2002. Frequency dispersion characteristics of phase velocities in surface wave for rotational components of seismic motion, *J. Sound Vibr.,* **258,** 815–827.

Li, H.-N., Sun, L.-Y. & Wang, S.-Y., 2001. Improved approach for obtaining rotational components of seismic motion, Translations SMiRT 16, Paper 2043.

McLeod, D.P., Stedman, G.E., Webb, T.H. & Schreiber, U., 1998. Comparison of standard and ring laser rotational seismograms, *Bull. seism. Soc. Am.,* **88,** 1495–1503.

Mikumo, T. & Aki, K., 1964. Determination of local phase velocity by intercomparison of seismograms from strain and pendulum instruments, *J. geophys. Res.,* **69,** 721–731.

Moriya, T. & Marumo, R., 1998. Design for rotation seismometer and their calibration, *Geophys. Bull. Hokkaido Univ.,* **61,** 99–106.

Niazi, M., 1986. Inferred displacements, velocities and rotations of a long rigid foundation located at El Centro differential array site during the 1979 Imperial Valley, California earthquake, *Earthquake Eng. Struct. Dyn.* **14,** 531–542.

Nigbor, R., 1994. Six-degree-of-freedom ground-motion measurement, *Bull. seism. Soc. Am.,* **84,** 1665–1669.

Oliveira, C.S. & Bolt, B.A., 1989. Rotational components of surface strong ground motion, Earthquake Eng. *Struct. Dyn.,* **18,** 517–526.

Pancha, A., Webb, T.H., Stedman, G.E., McLeod, D.P. & Schreiber, U., 2000. Ring laser detection of rotations from teleseismic waves, *Geophys. Res. Lett.,* **27,** 3553–3556.

Rautenberg, V., Plag, H.-P., Burns, M., Stedman, G.E. & Jüttner, H.-U., 1997. Tidally induced Sagnac signal in a ring laser, *Geophys. Res. Lett.,* **24,** 893–896.

Schreiber, K.U., Velikoseltsev, A., Rothacher, M., Klügel, T., Stedman, G.E. & Wiltshire, D.L., 2004. Direct measurement of diurnal polar motion by ring laser gyroscopes, *J. geophys. Res.,* **109,** doi:10.1029/ 2003JB002803, B06405.

Schreiber, K.U., Klügel, T. & Stedman, G.E., 2003a. Earth tide and tilt detection by a ring laser gyroscope, *J. geophys. Res.,* **108**(B2), 10.1029/2001JB000569.

Schreiber, K.U., Velikoseltsev, A., Stedman, G.E., Hurst, R.B. & Klügel, T., 2003b. New applications of very large ring lasers, in *Symposium Gyro Technology*, pp. 8.0–8.7, ed. Sorg, H.

Schreiber, U., Igel, H., Cochard, A., Velikoseltsev, A., Flaws, A., Schuberth, B., Drewitz, W. & Müller, F., 2005. The GEOsensor project: A new observable for seismology, in 'Observation of the System Earth from Space', Springer.

Schreiber, U., Stedman, G.E., Igel, H. & Flaws, A., 2006. Ring laser gyroscopes as rotation sensors for seismic wave studies, in '*Earthquake source asymmetry, structural media and rotation effects*' edsTeisseyre *et al.*, Springer Verlag.

Shearer, P.M., 1999. *Introduction to seismology*, Cambridge University Press.

Singh, S.K., Santoyo, M., Bodin, P. & Gomberg, J., 1997. Dynamic deformations of shallow sediments in the valley of Mexico, part II: Single station estimates, *Bull. seism. Soc. Am.,* **87,** 540–550.

Spudich, P., Steck, L.K., Hellweg, M., Fletcher, J.B. & Baker, L.M., 1995. Transient stresses at Parkfield, California, produced by the M7.4 Landers earthquake of June 28, 1992: observations from the UPSAR dense seismograph array, *J. geophys. Res.,* **100,** 675–690.

Stedman, G.E., 1997. Ring laser tests of fundamental physics and geophysics, *Reports Progr. Phys.,* **60,** 615–688.

Stedman, G.E., Li, Z. & Bilger, H.R., 1995. Sideband analysis and seismic detection in large ring lasers, *Appl. Opt.,* **34,** 7390–7396.

Suryanto, W., Igel. H., Wassermann, J., Cochard, A. & Schreiber, U., 2006a. Estimation of Love-wave dispersion from collocated measurements of translations and rotations Submitted to *Geophys. Res. Lett.*

Suryanto, W. et al., 2006b. First comparison of array-derived rotational ground motions with direct ring laser measurements, *Bull. seis. Soc. Am.,* in print.

Takeo, M. & Ito, H.M., 1997. What can be learned from rotational motions excited by earthquakes?, *Geophys. J. Int.,* **129,** 319–329.

Takeo, M., 1998. Ground rotational motions recorded in near-source region of earthquakes, *Geophys. Res. Lett.,* **25,** 789–792.

Teisseyre, R., Suchcicki, J., Teisseyre, K.P., Wiszniowski, J. & Palangio, P., 2003. Seismic rotation waves: basic elements of theory and recording, *Annals of Geophysics,* **46,** 671–685.

Trifunac, M.D. & Todorovska, M.I., 2001. A note on the usable dynamic range of accelerographs recording translation, *Soil Dyn. and Earth. Eng.,* **21**(4), 275–286.

Wielandt, E., 1993. Propagation and structural interpretation of non-plane waves, *Geophys. J. Int.,* **113,** 45–53.

Q7 Q8 Q9 Q10 Q11

QUERIES

Journal: GJI
Paper: gji3146

Dear Author

During the copy-editing of your paper, the following queries arose. Please respond to these by marking up your proofs with the necessary changes/additions. Please write your answers on the query sheet if there is insufficient space on the page proofs. Please write clearly and follow the conventions shown on the corrections sheet. If returning the proof by fax do not write too close to the paper's edge. Please remember that illegible mark-ups may delay publication.

Query Reference	Query	Remarks
Q1	Au: Reference Schreiber *et al.* (2005a,b) is not listed. Please check.	
Q2	Au: References Takeo *et al.* (1998) and Levevre (1993) are not listed. Please check.	
Q3	Au: Reference Takeo & Ito (1998) is not listed. Please check.	
Q4	Au: Please provide publisher location for Reference Aki & Richards (2002).	
Q5	Au: Please provide publisher location for Reference Cochard *et al.* (2006).	
Q6	Au: Please provide publisher location for Reference Kennett (2002).	
Q7	Au: Please provide publisher/location (if available) for Reference Schreiber *et al.* (2003b).	
Q8	Au: Please provide publisher location for Reference Schreiber *et al.* (2005).	
Q9	Au: Please list all editors if eight or fewer and provide editor initial(s) for Reference Schreiber *et al.* (2006).	
Q10	Au: Please provide publisher location for Reference Shearer (1999).	
Q11	Au: Please update References Suryanto *et al.* (2006a,b).	

MARKED PROOF

Please correct and return this set

Please use the proof correction marks shown below for all alterations and corrections. If you wish to return your proof by fax you should ensure that all amendments are written clearly in dark ink and are made well within the page margins.

Instruction to printer	*Textual mark*	*Marginal mark*
Leave unchanged	··· under matter to remain	Stet
Insert in text the matter indicated in the margin		New matter followed by 
Delete	 through matter to be deleted	
Delete and close up	 through matter to be deleted	
Substitute character or substitute part of one or more word(s)	/ through letter or  through word	New letter or new word
Change to italics	— under matter to be changed	
Change to capitals	 under matter to be changed	
Change to small capitals	under matter to be changed	
Change to bold type	under matter to be changed	
Change to bold italic	 under matter to be changed	
Change to lower case	Encircle matter to be changed	
Change italic to upright type	(As above)	
Insert 'superior' character	/ through character or  where required	 under character e.g. 
Insert 'inferior' character	(As above)	 over character e.g. 
Insert full stop	(As above)	
Insert comma	(As above)	
Insert single quotation marks	(As above)	and/or 
Insert double quotation marks	(As above)	and/or
Insert hyphen	(As above)	
Start new paragraph		
No new paragraph		
Transpose		
Close up	linking ⌢ letters	
Insert space between letters	 between letters affected	
Insert space between words	 between words affected	
Reduce space between letters	between letters affected	
Reduce space between words	between words affected	